*CATRINA* (2024), 33(1):-113-127


# Appraising the Impact of Land Cover Change on Divergences in LST, NDVI, and NDBI Using Landsat Satellite Data in North East Cairo, Egypt

**Marwa A. Mohamed[1*], Mohamed O. Arnous[2], Mohamed H. Geriesh[2], Hany F. Abdelgawad[1]**
[1] Geology Department, Faculty of Science, El-Arish University, Al-Arish 45511, North Sinai, Egypt.
[2] Geology Department, Faculty of Science, Suez Canal University.

Received: August 8, 2024; Accepted: August 21, 2024

## ABSTRACT

North East Cairo City (NECC), a relatively nascent urban area in Egypt, has experienced rapid expansion over recent decades. Understanding the environmental repercussions of land cover transformations in such regions has become increasingly paramount. This study investigates the intricate relationships between land cover change, NDBI, NDVI, and LST in NECC over twenty years (2000–2020) time span. We are employing a temporal series of Landsat imagery, including ETM+ and OLI/TIRS data, and sophisticated geospatial methodologies. The satellite imagery is classified into five distinct land cover categories: urban areas, bare land, agricultural areas, salinized soil, and water bodies. The findings indicate a significant increase in urban/built-up areas by approximately 211.2 km², accompanied by a concomitant decrease in bare land and agricultural areas by 196.2 km² and 23.9 km², respectively. Notably, the highest LST values were observed in bare land areas, escalating from 38–45°C in 2000 to 61–62°C in 2020, and in urban areas, rising from 36–37°C in 2000 to 60°C in 2020. The research revealed a pronounced correlation between the increase in built-up areas and the observed changes in LST, NDBI, and NDVI. Specifically, both NDBI and LST values exhibited an upward trend corresponding with the expansion of built-up areas. These results underscore the profound impact of urbanization on LST, offering critical insights into the consequential shifts in environmental indices. Furthermore, this study provides valuable guidance for sustainable urban planning practices in NECC, emphasizing the need for strategic interventions to mitigate the adverse effects of rapid urban expansion on the local climate and ecosystem.

**Keywords**: Geospatial analysis; Land use/Land cover; Land surface temperature; Normalized difference built-up index; Normalized difference vegetation index; Urban expansion.

## INTRODUCTION

In recent years, there has been an intensified focus on examining the dynamics of land cover (LC) transformations and their intricate interactions with a spectrum of biophysical environmental parameters. Scholars have meticulously concentrated on pivotal biophysical metrics such as land surface temperature (LST), normalized difference vegetation index (NDVI), and normalized difference built-up index (NDBI). These metrics are indispensable for monitoring LC alterations and evaluating the reciprocal influences between LC practices and climatic variables (Alademomi *et al*., 2020; Guha *et al*., 2020; Arnous and Mansour, 2023). The escalation of anthropogenic activities and urban sprawl globally has precipitated significant modifications in LC and vegetative patterns, thereby perturbing the equilibrium of natural ecosystems (Choudhury *et al*., 2019; Das *et al*., 2020).

Human populations have predominantly inhabited compact, rural communities. However, recent centuries have witnessed a significant demographic shift towards urbanization. This process is characterized by the growth in population density and spatial extent of urban areas, fundamentally transforming land use and land cover (LULC) patterns (Pal *et al*., 2017). According to projections by the United Nations, urbanization, coupled with the global population increase, is expected to add approximately 2.5 billion urban residents by 2050, with nearly 90% of this growth occurring in Asia and Africa (United Nations, 2014). The rapid increase in global population and economic development has led to significant changes in the Earth's land system (Bhanage *et al*., 2021). These LULC changes result from both natural processes and anthropogenic activities, reflecting a complex interplay that reshapes the Earth's surface. Historically, humans have modified landscapes to meet the demands for food, shelter, and other necessities. However, the current rate, scale, and intensity of these modifications are unprecedented (Gebreslassie, 2014; Hassan *et al*., 2016; Arnous and Green, 2015; Arnous *et al*., 2017; Lin *et al*., 2018). These transformations have profound impacts on various Earth system processes, including climate regulation, biodiversity conservation, hydrological cycles, ecosystem stability, forest health, and biogeochemical cycles (Jansen and Di Gregorio, 2002; Were *et al*., 2014; Lin *et al*., 2018). A major challenge arising from LULC changes is the increase in land surface temperatures, a phenomenon extensively documented in the literature (Mallick *et al*., 2008; Arnous and Mansour, 2023).

Land surface temperature (LST) is one of the main biophysical metrics for urban health assessments (Weng and Xiao, 2007). It is the temperature of the land's surface that is obtained from solar radiation

* *Corresponding author e-mail: marwam363@gmail.com.*

(Jaber, 2019). The term refers to the quantification of the perceived temperature of the Earth's surface at particular locations (Obiefuna *et al*., 2018), LST measurement has great importance in several domains, such as climatic variability and change, urban heat island influence, land/atmosphere observations, fire monitoring, mapping, detection of land cover change, geological investigations, agricultural management, and water management (Jaber, 2019; Arnous and Mansour 2023). LST may provide data on the physical attributes of the soil surface and atmospheric conditions, together with changes in land use and activities by humans that impact the climate (Fathizad *et al*., 2017). Because of the significant variety of LULC surfaces such as vegetation, surface roughness, topography, and soil, the LST varied fast in space as well as in time (Vauclin *et al*., 1982; Prata *et al*., 1995; Liu *et al*., 2006; Neteler, 2010). The impervious surfaces, such as buildings, roads, and industries, are known to serve land use purposes. These surfaces can absorb shortwave solar radiation, but they also contribute to a reduction in the emission of longwave terrestrial radiation. This reduction directly affects the LST (Das *et al*., 2020). The calculation of LST is complex because of the surface heterogeneity caused by various land cover types and mixed land users. The reason for this is that the emissivity of terrestrial surfaces exhibits significant variability and may vary considerably over short distances (Akinbobola, 2019). The different types of land cover have an impact on the characteristics and patterns of LST. Guha *et al*. 2020 concluded that changes in LST over the seasons are mostly influenced by factors such as vegetation and temperature. While it is acknowledged that plant cover has a mitigating effect on LST, different kinds of vegetation might vary in their capacity to lower surface temperatures. Trees mitigate surface and air temperature by shade, in addition to evapotranspiration (Alexander, 2020).

Furthermore, to understand environmental changes, it is critical to conduct efficient monitoring of the Normalized Difference Vegetation Index (NDVI), a spectral indicator used to identify and measure long-term variations in vegetation coverage and condition (Fathizad *et al*., 2017). NDVI, ranging from -1 to +1, shows the condition and amount of green plant covering and biomass, (Jaber, 2019) states that vegetation density and health may be determined by higher values approaching 1, whereas values of zero or below indicate scant or unhealthy vegetation on the ground and non-vegetated surfaces. These technologies have been extensively used in monitoring the timing of agricultural growth stages, categorizing different types of vegetation, and calculating various physical characteristics of vegetation.

The NDVI function values below 0.1 indicate barren landscapes consisting of rock, sand, or snow. Shrubs and meadows have intermediate values ranging from 0.2 to 0.3, whereas high values ranging from 0.6 to 0.8 indicate temperate and tropical forests. This scale is effectively used for crop monitoring to indicate to farmers the areas of their fields that currently exhibit thick, moderate, or sparse vegetation. Research has shown a logical correlation between NDVI and LST. (Fathizad *et al*., 2017; Jaber, 2019; Guha *et al*., 2020; Alademomi *et al*., 2020).

The Normalized Difference Built-up Index (NDBI) is a spectral index that quantifies urbanization and land cover changes within a given area. Empirical studies have demonstrated a significant correlation between NDBI and Land Surface Temperature (LST) (Choudhury *et al*., 2019; Das *et al*., 2020; Guha *et al*., 2020). Higher NDBI values, which range from -1 to +1, indicate increased impervious surface coverage, while lower values suggest more permeable surfaces. Locally, the expansion of built-up or impervious regions alters the geometric and physical properties of the land surface compared to natural land cover, impacting radiation budgets and surface energy dynamics (Choudhury *et al*., 2019). Specifically, impervious surfaces such as buildings, roads, and industrial sites enhance the absorption of shortwave radiation and reduce energy dissipation through longwave radiation emission (Choudhury *et al*., 2019; Das *et al*., 2020). Consequently, these impermeable surfaces exhibit higher Land Surface Temperatures (LST) compared to their surrounding environments. The Normalized Difference Built-up Index (NDBI), akin to other spectral indices that quantitatively characterize Land Use and Land Cover (LULC) types, has been extensively utilized in research investigating the relationship between LST and LULC. However, the variability in the correlation between LST and NDBI across different seasons remains a critical issue. NDBI holds significant importance in urban areas characterized by high population densities, as it provides essential insights into the extent of urbanization and its environmental impacts (Xiong *et al*., 2012; Guha *et al*., 2018).

Contemporary research has increasingly focused on understanding the patterns of land cover change and their relationship to various environmental conditions. Key environmental indicators, such as LST, NDVI, and NDBI, have garnered significant attention (Grigoraș and Urițescu, 2019; Jaber, 2019; Guha *et al*., 2020). Numerous studies have elucidated the relationship between LST and LULC, consistently revealing that changes in LULC, particularly in urban areas, result in elevated LST (Weng *et al*., 2004; Pal and Ziaul, 2017; Aboelnour and Engel, 2018). This growing body of research highlights the critical need for comprehensive analysis and strategic management of land cover changes to mitigate their adverse environmental impacts.

The North East of Cairo City (NECC), recognized as one of Egypt's most rapidly expanding regions, has experienced substantial anthropogenic activities and significant land use and land cover (LULC) transformations. This growth has led to the reclamation of vast areas and the establishment of new urban settlements such as El-Salaam, El-Obour, El-Sherouk, and Tenth of Ramadan. These developments have

precipitated numerous hydrogeological challenges, including dramatic alterations in land cover, shifts in land surface temperature, soil salinization, reduction in vegetative cover, and overall hydro-geoenvironmental degradation (Abdel Aleem, 2023; El-Rayes *et al.*, 2023). The goal of this initiative research is to execute the correlations amongst Land Surface Temperature (LST), Normalized Difference Vegetation Index (NDVI), Normalized Difference Built-up Index (NDBI), and alteration in land cover in North East Cairo City to provide insights into the urban heat island effect, inform environmental monitoring, and support sustainable urban planning in Northeast Cairo.

**Study area**

The North-East Cairo City (NECC) area, strategically positioned in the southeastern Nile Delta, encompasses portions of three governorates: El Sharkeya, El Qalyubia, and Cairo. This region spans an area of approximately 1428.54 km², delineated by latitudes 30° 8' to 30° 26' N and longitudes 31° 08' to 31° 44' E. The northern and northwestern boundaries are defined by the Ismailia Canal, Belbeis Drain, and adjacent agricultural lands. To the east, the area is bounded by the 10th of Ramadan City, while the southern periphery is demarcated by the Cairo-Suez Road. Significant landmarks within the southwestern sector include the Al Gabal Al Asfar drain, a sewage treatment plant, the Abu Zabal dumpsite, and the Ard El-Berka water station, primarily located in El-Salam City (Fig. 1).

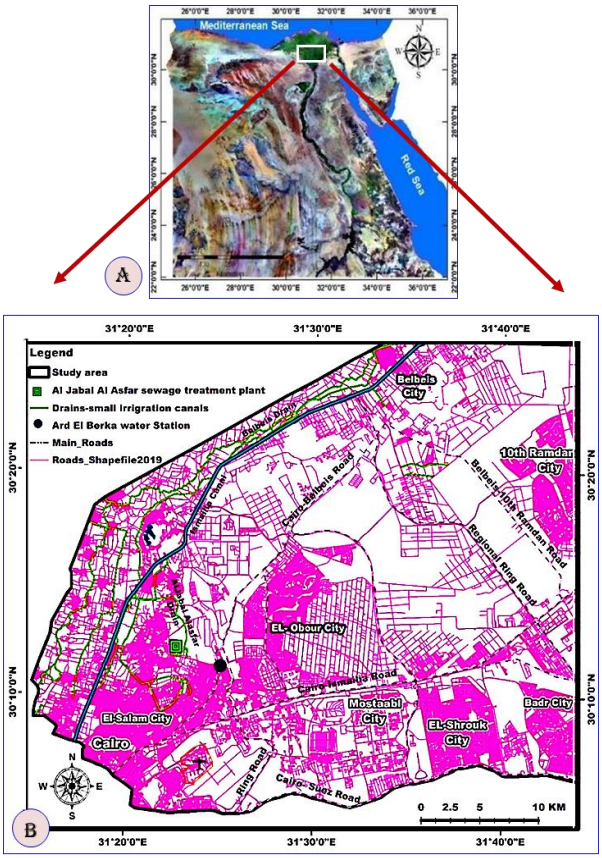


**Figure (1):** Satellite map of Egypt (a) showing the location of the study area and (b) the main cities and road network of the NECC area.

The influence of road networks on the magnitude, velocity, and direction of urban expansion is widely recognized (Shalaby *et al.*, 2022). In the context of the New Egyptian Capital City (NECC), a complex network of radial and ring roads has been systematically developed to support the infrastructure needs of rapidly growing urban settlements. The radial road system comprises key routes such as the 10th of Ramadan to Belbeis, Cairo to Suez, Cairo to Ismailia, and Cairo to Belbeis roads, facilitating seamless connectivity between NECC and Cairo City to the west, as well as major eastern governorates and districts, including Port Said, Ismailia, and Suez Cities, and the Suez Canal (Fig. 1). Complementing the radial roads, the NECC area is encircled by an array of ring roads, notably the Central Ring Road, the Middle Ring Road, and the Regional Ring Road. These arterial networks are pivotal in shaping the spatial dynamics and expansion trajectories of urban areas within NECC, underscoring the intrinsic link between infrastructural development and urbanization patterns. The strategic planning and implementation of these road networks not only facilitate efficient movement and connectivity but also significantly influence the region's urban morphology and growth prospects.

## MATERIALS AND METHODS

The Landsat program, a joint effort by the National Aeronautics and Space Administration (NASA) and the United States Geological Survey (USGS), has been monitoring the Earth through satellite missions since 1972 and provides free access to data on Earth's resources. We conducted our analysis using a time series of Landsat images captured by high-quality sensors, including Landsat Enhanced Thematic Mapper Plus (ETM+) and Landsat Operational Land Imager (OLI) / Thermal Infrared Sensor (TIRS) sensors. Only cloud-free satellite data was selected from the USGS website (https:/earthexplorer.usgs.gov) as a georeferenced dataset. The images were in UTM projection (WGS 84 datum, zone 36 N). Remote sensing data analysis was performed using several software tools; ERDAS Imagine was used for image processing including sub-setting, thematic map preparation, atmospheric, radiometric, and geometrical correction.

Image enhancement techniques, including contrast stretching, optimal band combination, and principal component analysis, are employed to generate high spectral resolution imagery. The ENVI 5.3 software is involved in performing the image classification of land use and land cover (LULC) as well as the development of change detection maps.

To produce various spectral indices and land surface temperature (LST) images, ArcGIS 10.5 was utilized. Subsequently, STATISTICA 7 is employed to carry out comprehensive statistical analyses. This multi-faceted approach ensured a robust and detailed examination of the data, providing significant insights into the spatial and temporal dynamics of the study area.

Figure (2) defines the comprehensive methodology employed to achieve the study's objectives. The multi-temporal data utilized comprises three complete scenes from each of the ETM+7, OLI+8, and TIRS+8 sensors, specifically corresponding to the Path/Row coordinates of 176/39. These scenes, captured in November and July, facilitated the assessment of NDBI and NDVI spectral indices, land use and land cover (LULC), and land surface temperature (LST), respectively. The data spans a twenty-year interval, covering the years 2000 and 2020. Detailed characteristics of the Landsat ETM+7 and OLI datasets are presented in Tables (1) and (2). Moreover, the Landsat imagery was synthesized into false color composites utilizing band combinations of (7, 4, 2) for Landsat 7 ETM + and (7, 5, 3) for Landsat 8 OLI, as depicted in Figures (3) and (4). These composites were further enhanced through pan-sharpening techniques employing the panchromatic band, thereby augmenting the spatial resolution and visual clarity of the image composites. This methodical approach ensured the precise analysis of temporal and spatial variations in the study area, facilitating a thorough evaluation of the environmental changes over the specified period.

**Land cover classification and land use change**

After pre-processing, the multi-spectral remotely sensed data are employing image classification techniques like supervised or unsupervised classification to classify the imagery from different periods into land cover classes and create LULC maps. In this work, a supervised approach for Maximum Likelihood (MLC) classification is used. MLC is the most often used supervised classification, which is utilized in a range of applications (Sisodia, *et al*., 2014, Arnous and Green 2015). In addition to outperforming the other known parametric classifications, MLC takes into account the variance-covariance within the class distributions (Erdas, 1999). The MLC classification method is often used to assign a pixel to a certain class based on its similarity to the target class (Ahmed and Ahmed 2012).

The main five signature classes were selected for classification urban area, agricultural land, bare land, salinized soil, and waterbodies. Residential buildings, highways, industries, and commercial buildings illustrate the urban area. The agricultural land represents both the areas with and without vegetation. The bare land represents the soil and unused land. Training areas have been developed by selecting one or more polygons for each class. Pixels were taken to be the training pixels for a specific class within the training area. Then, the Confusion Matrix Using Ground Truth ROIs in ENVI5.0 was utilized in this analysis to test the accuracy of the classification of maximum likelihood.

NDVI is an effective indicator of surface vegetation coverage and crop canopy growth stages. The temporal growth pattern of vegetation coverage, as expressed by NDVI, plays a crucial role in distinguishing crop types, although it may introduce some variation in values for certain crops. The most commonly used vegetation index is NDVI (Purevdorj *et al*., 1998; Arnous and Green, 2015). NDVI is calculated using visible and near-infrared (NIR) bands, which reflect vegetation health and density. It is determined by the difference between the reflected near-infrared and red band combinations. NDVI is computed as follows:

$$NDVI = \frac{(NIR - R)}{(NIR + R)}$$

Where R and NIR represent the red and near-infrared bands, respectively.

To delineate urban land from Landsat imagery, this study used the Normalized Difference Built-up Index.

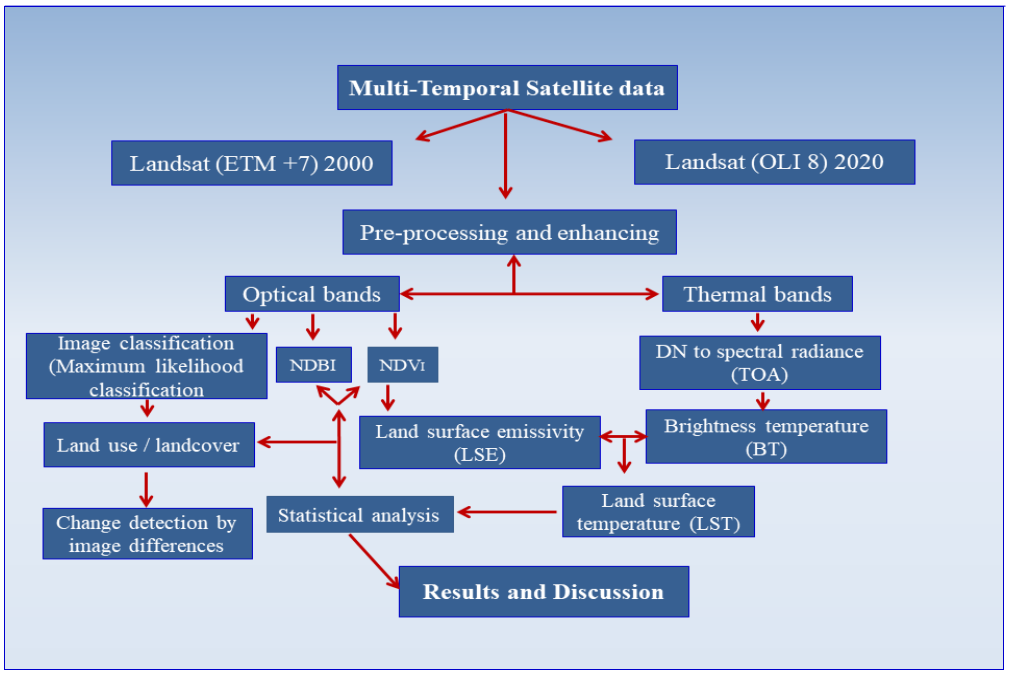


**Figure (2):** Methodological Framework for Multi-Temporal satellite data analysis

**Table (1):** Characteristics of Landsat ETM+7 data (NASA, 2003)

| Band No. | Wavelength interval (µm) | Spectral response | Resolution (m) |
|---|---|---|---|
| 1 | 0.45 - 0.52 | Blue-Green | 30 |
| 2 | 0.52 - 0.60 | Green | 30 |
| 3 | 0.63 - 0.69 | Red | 30 |
| 4 | 0.76 - 0.90 | Near IR | 30 |
| 5 | 1.55 - 1.75 | Mid-IR | 30 |
| 6 | 10.40 - 12.50 | Thermal IR | 60 |
| 7 | 2.08 - 2.35 | Mid-IR | 30 |
| 8 | 0.52 - 0.90 | Pan | 15 |

**Table (2):** Characteristics of Landsat 8 OLI data (NASA, 2013)

| Band No. | Wavelength interval (µm) | Spectral Response | Resolution (m) |
|---|---|---|---|
| 1 | 0.43 – 0.45 | Coastal/Aerosol | 30 |
| 2 | 0.45 - 0.52 | Blue-Green | 30 |
| 3 | 0.52 - 0.60 | Green | 30 |
| 4 | 0.63 - 0.69 | Red | 30 |
| 5 | 0.84 - 0.88 | Near IR | 30 |
| 6 | 1.56 - 1.66 | SWIR-1 | 30 |
| 7 | 2.10 – 2.30 | SWIR-2 | 30 |
| 8 | 0.50 – 0.68 | Pan | 15 |
| 9 | 1.36 – 1.39 | Cirrus | 30 |
| 10 | 10.30 – 11.30 | Thermal IR-1 | 100 |
| 11 | 11.50 – 12.50 | Thermal IR-2 | 100 |

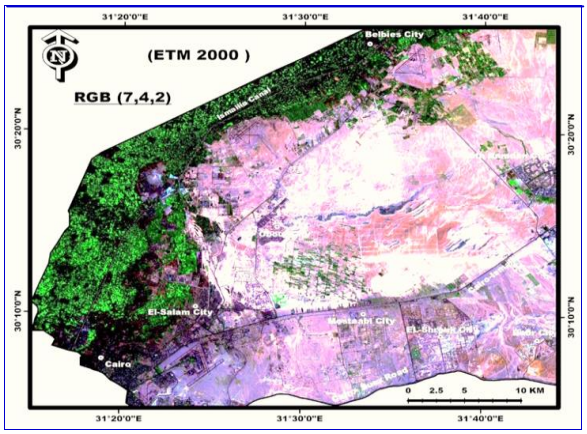


**Figure (3):** Landsat ETM+7 image of the year (2000) for the study area.

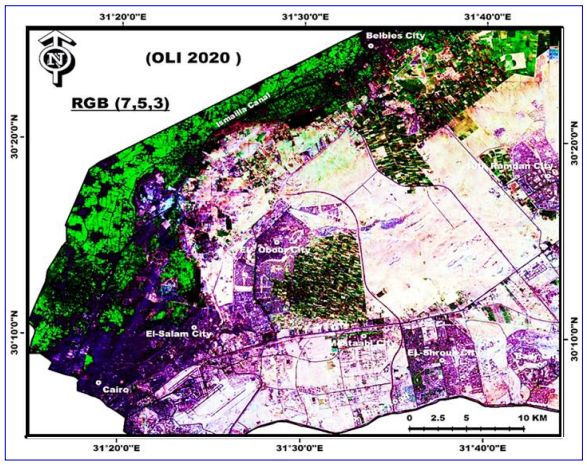


**Figure (4):** Landsat 8 OLI satellite image of the year (2020) that is used for conducting image processing.

(NDBI) as introduced by Zhao and Chen (2005). The NDBI is particularly sensitive to the presence of built-up areas. It is derived using specific spectral bands to identify and quantify these regions by analyzing the spectral characteristics of various land use/land cover (LU/LC) classes. The NDBI is calculated using the following formula:

$$NDBI = \frac{[(band\ 5) - (band\ 4)}{[(band\ 5 + (band\ 4)]}$$

Where, Bands 4 and 5 correspond to the Landsat TM or ETM+ images.

In the current study, the NDBI for Landsat 8 imagery is computed using the formula:

$$NDBI = \frac{[(band\ 6) - (band\ 5)}{[(band\ 6 + (band\ 4)]}$$

where Bands 5 and 6 pertain to the Landsat 8 sensor (Arnous and Green, 2015). This index effectively distinguishes built-up areas from other land cover types, providing a robust tool for urban land extraction and analysis.

**Land surface temperature (LST) estimation**

To derive Land surface temperature (LST) readings from Landsat 7 and Landsat 8 satellite imagery, a meticulous four-step process must be followed. It is imperative to acknowledge that while the initial step diverges between the two satellites, the subsequent three steps remain consistent for both. The derivation of LST from the thermal bands of satellite imagery necessitates the utilization of specific bands or algorithms. Specifically, the thermal infrared bands employed for LST determination are band 6 for ETM+7 data, and bands 10 and 11 for TIRS+8, which measure the quantity of infrared radiation emitted from various land surfaces. Each band pixel contains a digital number (DN) value, representing a raw measure acquired by the sensor. Consequently, these DN values must be converted into physical quantities, such as radiance and brightness temperature, to extract quantitative information from the raw satellite data (Arnous and Mansour, 2023).

The final land surface temperature (LST) map is generated through a series of sequential steps: first, the computation of the Normalized Difference Vegetation Index (NDVI); second, the conversion of Thermal Infrared Sensor (TIRS) band data to top-of-atmosphere (TOA) spectral radiance; and third, the estimation of atmospheric brightness temperature. Finally, the LST values are converted from Kelvin (K) to degrees Celsius (°C) (Khyami, 2021). These methodological steps are supported by equations detailed in Table (3). Follo-wing these procedures, LST is extracted, measured, and mapped from the thermal bands of remote sensing satellite data. This approach enhances the accuracy of temperature estimations and facilitates the analysis of spatiotemporal variations in LST patterns. In addition, the statistical correlation analyses are performed to investigate the interrelationships between NDVI, the NDBI, land use/land cover (LULC) changes, and LST, providing deeper insights into urban heat dynamics and environmental variability.

**Table (3):** Estimated parameters and mathematical formulas for remote sensing-based land surface analysis.

| Estimated Parameter | Mathematical formula | Reference |
|---|---|---|
| **NDBI** | $NDBI = \frac{SWIR - NIR}{SWIR + NIR}$ | Zha *et al.* (2003) |
| **NDVI** | $NDVI = \frac{(NIR - R)}{(NIR + R)}$ | Liu *et al*. (2018) |
| **DN to TOA** | | |
| **Landsat7** | $L\lambda = \frac{L_{max}\ L_{min}}{QCAL_{MAX} - QCAL_{MIN}} X(QCAL - QCAL_{MIN}) + L_{MIN}$ | Chander and Markham (2003) |
| **Landsat8** | $L\lambda = ML\ X\ QCAL + AL$ | USGS (2014) |
| **TOA to BT** | $T_b = \frac{K2}{In\left(\frac{(K1)}{L\lambda}\right)+1)}$ | Chander *et al.* (2009) |
| **LSE** | $PV = \left(\frac{(NDVI - NDVI\,min}{NDVI\,max + NDVI\,min}\right)^2$<br>$E = 0.0004 \times PV + 0.986$ | Xiaolei *et al.* (2013) |
| **LST** | $LST = \frac{T_K}{1 + (\frac{(\lambda TK1)}{p}) ln\,\varepsilon}$ | Jeevalakshmi *et al*. (2017) |

NDBI, Normalized Difference Built-up Index; NDVI, Normalized Difference Vegetation Index; BT, Brightness Temperature LSE, Land Surface Emissivity; LST, Land Surface Temperature

## RESULTS

This study investigated the spatial and temporal relationships between Land Surface Temperature (LST), Normalized Difference Vegetation Index (NDVI), Normalized Difference Built-up Index (NDBI), and Land Cover (LC) changes. To elucidate the interrelationships among these biophysical environmental parameters, we utilized a suite of geospatial thematic maps for each parameter. Overlay analysis is employed to detect patterns of interrelationships. Furthermore, statistical techniques, including correlation analysis, were applied to quantify the strength and direction of these relationships, providing a robust assessment of their interconnected dynamics.

### Analysis of land use/land cover changes and detection

Figures (5) and (6) illustrate the land use and land cover (LU-LC) maps, along with the rates of LU-LC changes in North East Cairo City (NECC) over a 20-year period (2000–2020). The data presented in Table (4) indicate a significant expansion of urban areas, which increased from 165.7 km² in 2000 to 376.9 km² in 2020, resulting in a net gain of 211.2 km². This expansion corresponds to an average annual growth rate of 10.56 km² per year, highlighting the rapid urbanization in the study area. Agricultural cover also declined from 297.4 km² in 2000 to 273.5 km² in 2020, with a net decrease of 23.9 km² at an annual rate of -1.195 km²/year.

Waterlogging exhibited a modest increase from 2.3 km² in 2000 to 3.4 km² in 2020, reflecting a net gain of 1.1 km² at an annual rate of 0.055 km² per year. Similarly, salinized areas expanded from 2.5 km² in 2000 to 5.3 km² in 2020, representing an increase of 2.8 km² at an annual rate of 0.14 km² per year. Remarkably, the water body area expanded significantly, increasing from 0.2 km² in 2000 to 5.2 km² in 2020, resulting in a total gain of 5 km² at an annual rate of 0.25 km² per year.

The classification results for the NECC area in 2000 and 2020 revealed that bare land was the most dominant land cover class, constituting 64.96% in 2000 and 51% in 2020, followed by agricultural land, which decreased from 20.9% in 2000 to 19% in 2020. In contrast, water bodies and salinized soils showed slight increases, from 0.01% to 10.37% and from 0.17% to 0.37%, respectively. Urban areas exhibited a significant increase, from 11.64% in 2000 to 27% in 2020 (Figure 7). Furthermore, the land cover classification accuracy was validated through accuracy assessment analysis, yielding accuracy values of 93.33% for the year 2000 and 96.67% for the year 2020. The overall accuracy was lowest in 2000 and highest in 2020, likely due to the superior quality of Landsat 8 OLI images compared to Landsat 7 ETM+ images.

### Analysis of variation in NDBI, NDVI, and LST

The analysis of urban boundaries (cities and settlement areas) using NDBI and multi-temporal images revealed that the study area underwent significant urban expansion from 2000 to 2020 (Fig. 8A-B). In the year 2000, urban areas appeared in red in the North East Cairo City (NECC) with NDBI values approximately ranging from 0.08 to 0.2. Waterlogged areas and surface water vegetation, depicted in green, exhibited values between -0.06 and 0.08, dense vegetation, shown in dark green, had values between -0.03 and -0.06, and bare land, shown in pale green, had values ranging from 0.2 to 0.5.

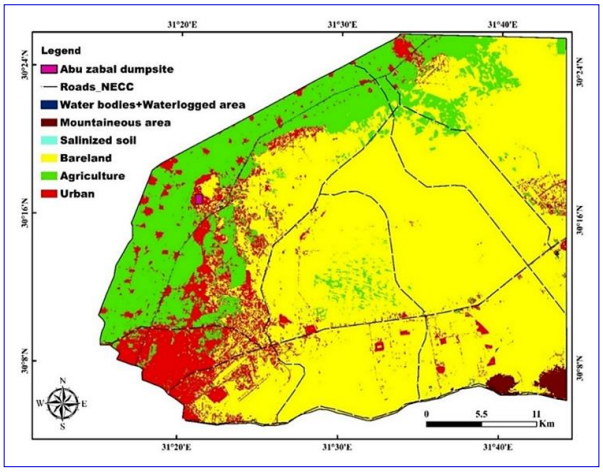


**Figure (5):** Supervised LULC classified Landsat image 2000 showing geospatial distribution for each type of classes within the NECC area.

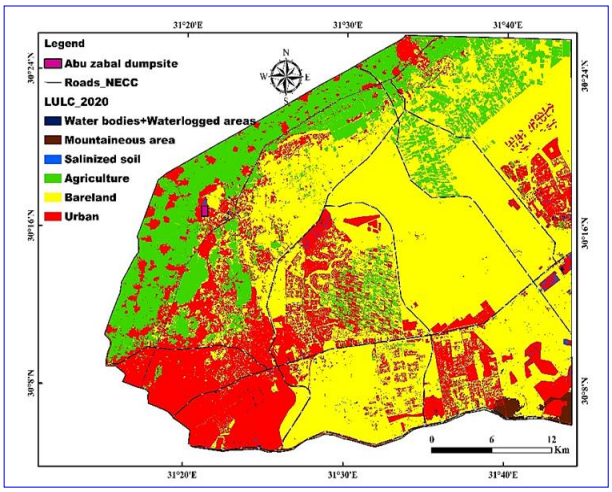


**Figure (6**): Supervised LULC classified Landsat image 2020 showing geospatial distribution for each type of classes within the NECC area.

By 2020, urban areas were indicated in red with NDBI values between -0.03 and 0.02. Waterlogged areas and surface water vegetation, still shown in green, had values between -0.1 and -0.03, dense vegetation, depicted in dark green, had values between -0.3 and 0.1, and bare land, shown in pale green, had values ranging from 0.02 to -0.3 (Table 5). The drivers of this urban expansion included the increasing population and the sustainable development projects initiated over the past three decades, aimed at fostering agricultural, economic, and technological development (Arnous and Green, 2015; Arnous *et al*., 2017; Moubarak, 2021; El-Rayes *et al*., 2023; Darwish,2024).

The NDVI rate was calculated using a raster calculator in ArcGIS over a twenty-year timespan, comparing the years 2000 and 2020. The analysis utilized ETM Landsat 7 imagery for 2000 and OLI Landsat 8 imagery for 2020 (Fig. 9A-B). In the year 2000, NDVI values ranged from -0.9 to 0.9. These values were classified into four categories: surface water and waterlogged areas (blue) with values from -0.9 to 0, bare land and urban areas (yellow) with values from 0 to 0.2, sparse vegetation (light green) with values from 0.3 to 0.4, and dense vegetation (dark green) with values from 0.5 to 0.9. In contrast, the NDVI values for year 2020 ranged from -0.1 to 0.6. These values were also classified into four categories: surface water and waterlogged areas (blue) with values from -0.1 to 0, bare land and urban areas (yellow) with values from 0 to 0.1, sparse vegetation (light green) with values from 0.2 to 0.4, and dense vegetation (dark green) with values from 0.5 to 0.6 (Table 6). This indicated an increase in vegetation cover and land reclamation in most of the investigated area, particularly in the northwest 10th of Ramadan area and the Orabi organization east of El-Obour City. In these regions, new irrigation wells and canals connected to the Ismailia canal had been constructed. However, there

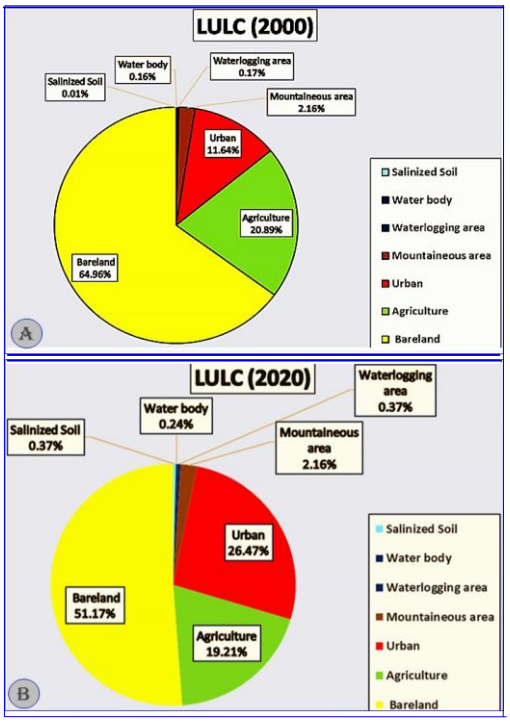


**Figure (7):** Pie chart showing the percentage change in LU/LC class categories within the NECC area between 2000 and 2020.

**Table (4):** Areal Distribution, Percentage, and Rate of Change of Different LULC Classes from 2000 to 2020**.**

| Class | LULC_2000 in Km2 | LULC_2000 in % | LULC_2020 in Km2 | LULC_2020 in % | Change in area km2 | Rate of change per year |
|---|---|---|---|---|---|---|
| **Urban** | 165.7 | 11.64% | 376.9 | 26.47% | 211.2 | 10.56 |
| **Bare land** | 924.7 | 64.96% | 728.5 | 51.17% | -196.2 | -9.81 |
| **Agriculture** | 297.4 | 20.89% | 273.5 | 19.21% | -23.9 | -1.195 |
| **Salinized area** | 2.5 | 0.17% | 5.3 | 0.37% | 5 | 0.25 |
| **Waterbody** | 0.2 | 0.01% | 5.2 | 0.37% | 1.1 | 0.055 |
| **Waterlogging area** | 2.3 | 0.16% | 3.4 | 0.24% | 2.8 | 0.14 |

**Table (5):** Normalized Difference Built-up Index (NDBI) spectral value ranges of different LULC classes in Landsat ETM+ (2000) and OLI (2020) Images.

| LULC Class | Color | ETM Landsat 7 image (2000) | OLI Landsat 8 image (2020) |
|---|---|---|---|
| | | Values range | Values range |
| **Urban area** | Red | 0.08 - 0.2 | 0.30 - 0.02 |
| **Waterlogged, Surface water** | Green | - 0.06 - 0.08 | -0.10 - 0.03 |
| **Dense vegetation** | Dark green | 0.03 -0.07 | -0.30 - 0.10 |
| **Bare land** | Pale green | 0.20 -0.50 | 0.20 - 0.30 |

**Table (6):** Normalized difference vegetation index (NDBI) spectral value ranges of different LULC classes in Landsat ETM+ (2000) and OLI (2020) Images.

| LULC Class | Color | ETM Landsat 7 image (2000) | OLI Landsat 8 image (2020) |
|---|---|---|---|
| | | Values range | Values range |
| **Surface water and waterlogged area** | Blue | -0.9 -0.0 | -0.1 - 0.0 |
| **Bare land - urban area** | Yellow | 0.0 - 0.2 | 0.0 - 0.1 |
| **Spare vegetation** | Light green | 0.3 -0.4 | 0.2 -0.4 |
| **Dense vegetation** | Dark green | 0.5 -0.6 | 0.5 -0.6 |

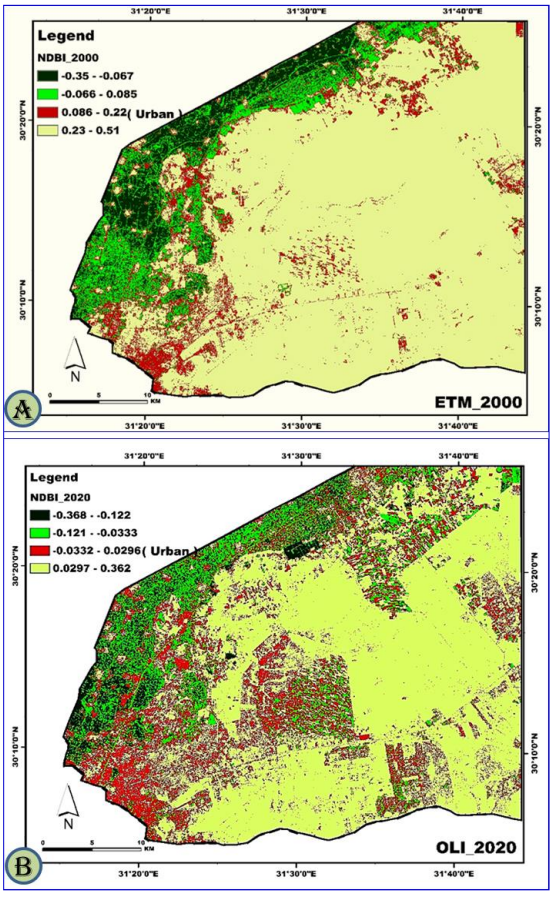


**Figure (8A-B)**: NDBI enhanced multi-temporal Landsat images of NECC showing the change in urbanized areas. A, Landsat images (2000); B, Landsat images (2020).

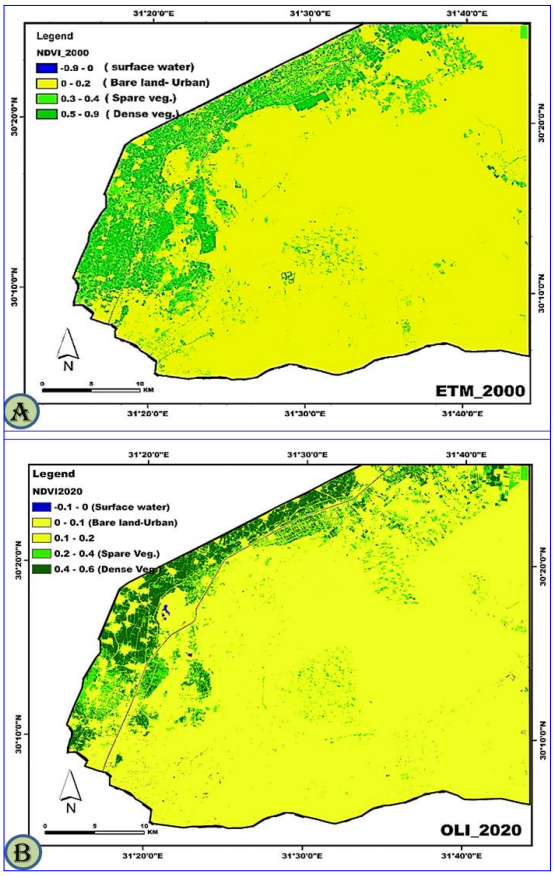


**Figure (9A-B):** NDVI enhanced ETM and OLI Landsat image of NECC area; showing the change of vegetation covers, land reclamation, surface water, and waterlogged area. A, ETM Landsat image of NECC area (2000); B, OLI Landsat image of NECC area (2020).

was a noticeable decrease in bare land (red) and an increase in surface water and waterlogged areas, although this was not consistently detected across all areas.

The analysis of LST distribution between 2000 and 2020, as depicted in Figure (10A-B), reveals significant shifts in LULC and LST. The LST analysis, detailed in Table (7), indicates that barren regions exhibit the highest temperatures, followed sequentially by built-up areas, agricultural lands, and water bodies. Specifically, in 2000, the LST in waterbody areas ranged from 32°C to 35°C, represented by a light green color. By 2020, these values increased to a range of 56°C to 58°C, depicted by a dark green color.

Agricultural areas displayed a varied trend, with LST values of 27°C to 31°C in 2000, rising to 59°C in 2020, attributed to the expansion of urban and barren lands, which consequently reduced vegetation cover. The LULC mapping and change estimation further

corroborate these findings. By comparing classified LULC maps from different time periods, areas undergoing significant change, such as the conversion of vegetation to urban landscapes, can be identified. This conversion has notably impacted LST, NDBI, and NDVI, highlighting the interplay between urbanization and environmental factors.

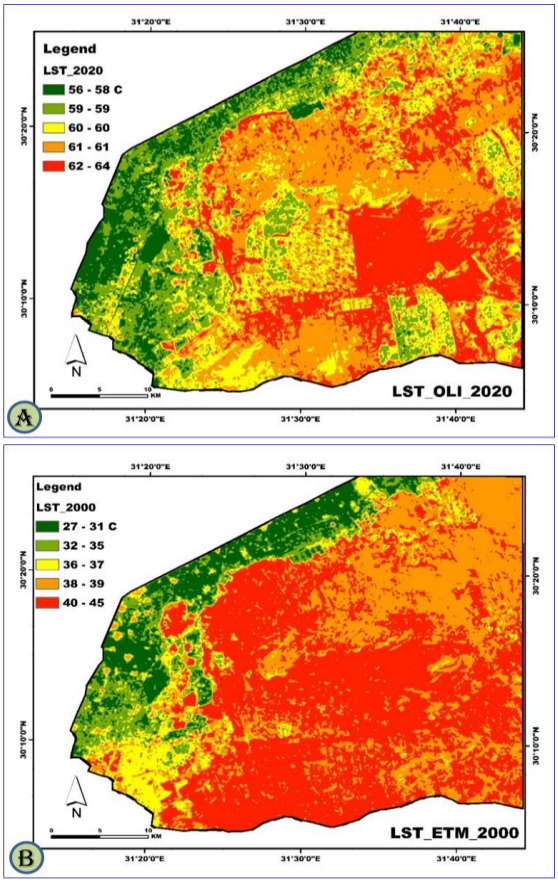


**Figure (10A-B):** Spatial pattern LST distribution maps for year 2000 (A) and 2020 (B) of NECC

## Interrelationship between LST, NDVI, and NDBI

To elucidate the intricate relationship between LST, NDBI, and NDVI, a statistical analysis was undertaken. Table (8) presents a detailed summary of the minimum, maximum, and means values across the NECC area, while Table (9) elaborates on the correlation coefficients for LST, NDBI, and NDVI for the years 2000 and 2020. The empirical findings indicated a robust positive correlation between LST and NDBI, with correlation values spanning from 0.74 to 0.99 across the analyzed periods. This pronounced positive correlation is visually corroborated by the 2D scatterplots in Figures (13) and (14). Conversely, the analysis revealed a significant negative correlation between NDVI and LST, underscoring those areas with denser vegetation exhibited lower surface temperatures. These results elucidate those urban areas, characterized by elevated NDBI values, experienced heightened temperatures, whereas vegetated regions, denoted by higher NDVI values, maintained cooler surface temperatures. The persistent positive correlation between LST and NDBI from 2000 to 2020 underscores the profound impact of urbanization on local climate dynamics, thereby accentuating the critical necessity of integrating vegetation into urban planning frameworks to ameliorate rising temperatures.

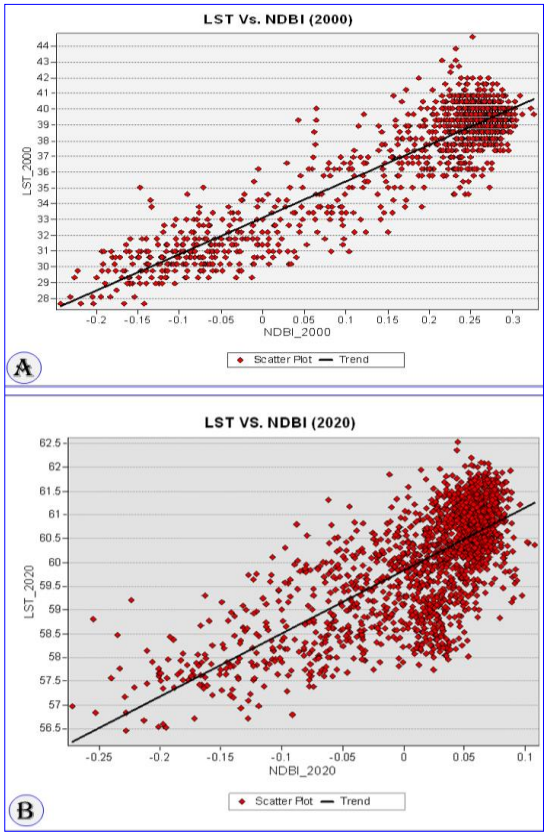


**Figure (11A-B):** Scatter plot show the relationship between LST, NDBI in year 2000 (A) and 2020 (B).

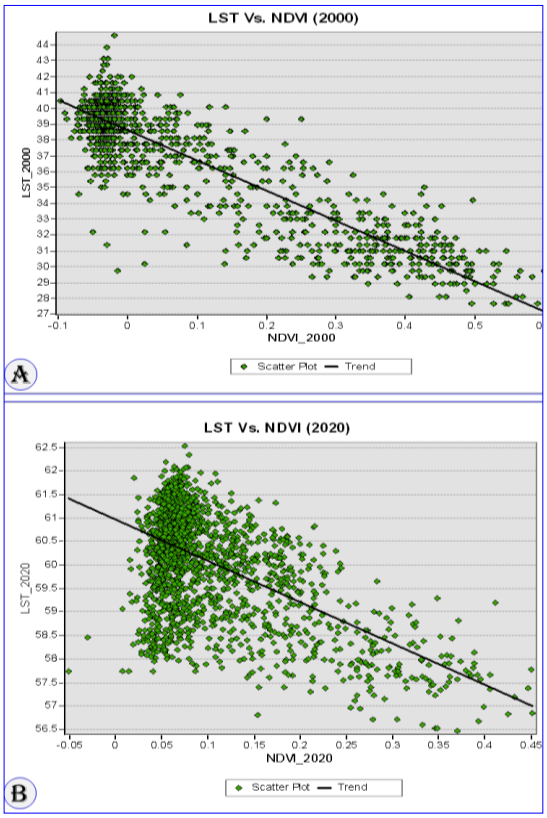


**Figure (14):** Scatter plot shows the relationship between LST, NDVI year 2000 (A) and 2020 (B).

**Table (7):** Change in LST (2000-2020) concerning LU/LC classes.

| LULC classes | Change in area km$^2$ | LST (2000) | LST (2020) |
|---|---|---|---|
| **Urban** | 211.2 | 36 ˚C -37 ˚C | 60 ˚C |
| **Bare land** | -196.2 | 38˚C- 45 ˚C | 61 ˚C |
| **Agriculture** | -23.9 | 27 ˚C-31 ˚C | 59 ˚C |
| **Water bodies** | 3.9 | 32 ˚C-35 ˚C | 58 ˚C -56 ˚C |

**Table (8):** Descriptive statistics of the Normalized Difference Vegetation Index (NDVI), Normalized Difference Built-up Index (NDBI), and Land Surface Temperature (LST).

| Measurement | LST 2000 | NDVI 2000 | NDBI 2000 | LST 2020 | NDVI 2020 | NDBI 2020 |
|---|---|---|---|---|---|---|
| **Maximum** | 44.61 | 0.6 | 0.33 | 62.54 | 0.45 | 0.11 |
| **Minimum** | 27.67 | 0.01 | 0.08 | 56.47 | 0.07 | 0.03 |
| **Mean** | 37.79 | 0.04 | 0.20 | 60.09 | 0.10 | 0.02 |
| **Sum** | 74217.99 | 82.89 | 395.87 | 118025.8 | 195.48 | 39.3 |
| **Standard Deviation** | 3.18 | 0.15 | 0.13 | 1.14 | 0.07 | 0.06 |
| **Nulls** | 0.0 | 0.0 | 0.0 | 0.0 | 0.0 | 0.0 |
| **Count** | 1964 | 1964 | 1964 | 1964 | 1964 | 1964 |

**Table (9):** Statistical correlation matrix of Land Surface Temperature (LST), Normalized Difference Vegetation Index (NDVI), and Normalized Difference Built-up Index (NDBI) for 2000 and 2020

| Parameter | LST 2000 | NDVI 2000 | NDBI 2000 | LST 2020 | NDVI 2020 | NDBI 2020 |
|---|---|---|---|---|---|---|
| **LST 2000** | 1 | | | | | |
| **NDVI 2000** | 0.831$^{*}$ | 1 | | | | |
| **NDBI 2000** | 0.991$^{**}$ | 0.898$^{**}$ | 1 | | | |
| **LST 2020** | 1.00$^{**}$ | 0.831$^{*}$ | 0.991$^{**}$ | 1 | | |
| **NDVI 2020** | 0.845$^{*}$ | 1.00$^{**}$ | 0.909$^{**}$ | 0.846$^{*}$ | 1 | |
| **NDBI 2020** | 0.741 | 0.989$^{**}$ | 0.824$^{*}$ | 0.741 | 0.985$^{**}$ | 1 |

*, highly positive correlation; **, very high positive correlation

## DISCUSSION

By reviewing the land use and land cover (LULC) changes and the statistical analysis, this investigation highlights the inter-relationship between urban expansion and environmental parameters in the NECC study area. It also, examines the spatial and temporal distribution of Land Surface Temperature (LST), Normalized Difference Vegetation Index (NDVI), and Normalized Difference Built-up Index (NDBI) in North East Cairo City (NECC) during a period of twenty years, from 2000 to 2020.

The NECC witnessed urban growth, with urban areas increasing by 211.2 km² at an average annual pace of +10.56 km². This urban growth has profoundly altered the landscape, resulting in an obvious decrease in the area of bare land and agriculture. To be more specific, the area of bare land declined by 196.2 Km$^2$, while the agricultural land declined by 23.9 Km$^2$. Conversely, slight rises were observed in water bodies and salinized areas, which indicates the continuous alterations in land use dynamics. According to the land use classification findings from 2000 and 2020, bare land and agricultural cover are the most prevalent categories of land use, even though their proportions have decreased over time. Urban areas have expanded significantly from 11.64% in 2000 to 27% in 2020, This shift underscores a distinct pattern and a clear trend of urban development and land conversion that are influenced by economic and demographic factors.

However, the LST analysis demonstrates a significant rise in surface temperatures, particularly in urban and bare land areas. The urban areas in 2020 recorded the highest Land Surface Temperature (LST) values, with temperatures ranging from 56-58°C. Compared to that, agricultural areas experienced lower temperatures, ranging from 27-31°C, while water bodies had temperatures ranging from 32-35°C. The primary contributing factor to this increase in temperature is mostly due to the widespread urbanization and decrease in vegetation cover.

The notable rise in temperature in urban areas highlights the Urban Heat Island (UHI) phenomenon, wherein the constructed environment absorbs and retains heat to a greater extent than natural landscapes. The finding matches up with previous studies that document the heat retention properties of metropolitan areas and the resulting influence on the local climate. The worldwide and Egyptian research extensively supports the strong correlation between urban expansion and the rise in land surface temperature (LST). Global research, notably studies conducted by Oke (1982), Weng *et al.* (2004), and Meng *et al.* (2010), emphasize that urbanization increases land surface temperature (LST) as a result of heat absorption by impermeable surfaces and decreased vegetation. In Egypt, academics Abd-Elmabod *et al.* (2022), and Mostafa *et al.* (2023) have observed notable increases in Land Surface Temperature (LST) due to the rapid expansion of urban areas and changes

in land cover. These findings align with global patterns and highlight how urban sprawl and material conductivity contribute to the intensification of the Urban Heat Island (UHI) effect.

The statistical analysis reveals a strong positive correlation between Land Surface Temperature (LST) and the Normalized Difference Built-Up Index (NDBI), with coefficients ranging from 0.74 to 0.99, indicating that increased built-up areas correspond to higher temperatures. Conversely, the correlation between the Normalized Difference Vegetation Index (NDVI) and LST is negative, signifying that denser vegetation is linked to cooler temperatures. This highlights the cooling effect of vegetation, which mitigates temperature increases associated with urbanization. The findings underscore the importance of maintaining and expanding green spaces to counteract the Urban Heat Island (UHI) effect and improve urban environmental quality, suggesting that green infrastructure is crucial for managing urban heat and enhancing climate resilience.

As an Overall implication, the study's results underscore the profound impact of urban expansion on LST, NDVI, and NDBI. The observed trends indicate that increasing built-up areas are the primary driver of higher surface temperatures, while the loss of vegetation exacerbates this effect. The study highlights the need for sustainable urban planning that integrates green spaces and environmental considerations to mitigate the negative impacts of urban heat. Effective urban planning and policy measures should focus on balancing development with environmental presservation. Strategies such as increasing green spaces, promoting sustainable construction practices, and enhancing urban greenery can help mitigate the UHI effect and promote a more sustainable urban environment. In conclusion, this study provides a comprehensive understanding of the interrelationships between LST, NDVI, and NDBI in the context of rapid urban expansion in the NECC. The findings underscore the need for integrated urban planning approaches that consider environmental impacts and promote sustainability. By addressing these issues, cities can better manage the challenges of urbanization and work towards creating more resilient and livable urban environments.

## CONCLUSION

This research reveals an extensive analysis of the linkages amongst Land Surface Temperature (LST), Normalized Difference Vegetation Index (NDVI), and Normalized Difference Built-Up Index (NDBI) in North East Cairo City (NECC) over twenty years (2000-2020). While agriculture and bare areas have reduced, there has been a noticeable increase in urban growth, which has led to a significant rise in land surface temperatures. The results emphasize that urban areas have greater temperatures than the adjacent natural landscapes. The study's observation indicates that urban areas exhibited the highest Land Surface Temperature (LST) readings, while agricultural areas and water bodies displayed comparatively lower temperatures. The robust positive association between Land Surface Temperature (LST) and Normalized Difference Built-up Index (NDBI) underscores the role of expanded urban areas in rising temperatures. Conversely, the negative correlation between the Normalized Difference Vegetation Index (NDVI) and LST underscores the cooling impact of vegetation. The findings line up with investigations conducted at both global and local levels, reinforcing the correlation between urbanization, and land surface temperature. The study's results align with the existing research that shows how urban expansion results in increased Land Surface Temperature (LST) as a result of heat absorption by impermeable surfaces and a reduction in vegetation. Based on these findings, the research promotes the implementation of sustainable urban planning that integrates green infrastructure and environmental factors. Efficient strategies should involve the enlargement of green areas, implementation of sustainable construction methods, and improvement of urban vegetation. Implementing such solutions is essential for reducing the land surface temperature and enhancing the quality of the urban environment, eventually promoting a more robust and livable environment in cities. Finally, this research emphasizes the critical need for integrated urban planning strategies that effectively harmonize development with environmental sustainability. By intelligently establishing and sustaining green infrastructure, where cities can successfully tackle the difficulties brought about by fast urban expansion, such as with higher land surface temperature, and improve the overall quality of urban life. This approach contributes to creating a more sustainable future for cities.

## REFERENCES

ABDELALEEM, M. 2023. Implication of land use changes on the groundwater flow regime and quality, North East Cairo, Egypt using geographic information systems (GIS), PhD, Suez Canal University, Ismailia, Egypt, 236 p.

ABD-ELMABOD, S.K., M.A. JIMÉNEZ-GONZÁLEZ, A. JORDÁN, Z. ZHANG, E.S. MOHAMED, A.A. HAMMAM, A.A. EL BARO-UDY, M.K. ABDEL-FATTAH, M.A. ABDELF-ATTAH, AND L. JONES. 2022. Past and future impacts of urbanisation on land surface temperature in Greater Cairo over a 45 year period. The Egyptian Journal of Remote Sensing and Space Science 25 (4): 961-974. https://doi.org/10.1-016/j.ejrs.2022.10.001.

ABOELNOUR, M., AND B. A. ENGEL. 2018. Application of remote sensing techniques and geographic information systems to analyze land surface temperature in response to land use/land cover change in Greater Cairo Region, Egypt. Journal of Geographic Information System, 10(1): 57-88.https://doi.org/10.4236/jgis.2018.101003.

AHMED, B., AND R. AHMED. 2012. Modeling urban land cover growth dynamics using multi-temporal

satellite images: A case study of Dhaka, Bangladesh. ISPRS International Journal of Geo-Information, 1:3–31. https://doi.org/10.3390/ijg-i1010003

AKINBOBOLA, A. 2019. Simulating land cover changes and their impacts on land surface temperature in Onitsha, South East Nigeria. Atmospheric and Climate Sciences, 9(02): 243. https://doi.org/10.4236/acs.2019.92015.

ALADEMOMI, A. S., C. J. OKOLIE, O. E. DARA-MOLA, R. O. AGBOOLA, AND T. J. SALAMI. 2020. Assessing the relationship of LST, NDVI, and EVI with land cover changes in the Lagos Lagoon environment. Quaestiones Geographicae, 39(3): 111-123. https://doi.org/10.2-478/quageo-2020-0025.

ALEXANDER, C. 2020. Normalized difference spectral indices and urban land cover as indicators of land surface temperature (LST). International Journal of Applied Earth Observation and Geoinformation, 86: 102013. https://doi.org/10.1-016/j.jag.2019.102013.

ARNOUS, M.O., A.E. EL-RAYES, AND A.M. HELMY. 2017. Land-use/land-cover change: A key to understanding land degradation and relating environmental impacts in Northwestern Sinai, Egypt. Environmental Earth Sciences, 76(7): 26. https://doi.org/10.1007/s12665-017-6571-3

ARNOUS, M.O., AND B.M. MANSOUR. 2023. Utilizing multi-temporal thermal data to assess environmental land degradation impacts: Example from Suez Canal region, Egypt. Environmental Science and Pollution Research, 30(1): 2145-2163. https://doi.org/10.1007/s11356-022-22237-z

ARNOUS, M.O., A.E. EL-RAYES, AND D.R. GREEN. 2015. Hydrosalinity and environmental land degradation assessment of the East Nile Delta region, Egypt. Journal of Coastal Conservation, 19(4): 491–513. https://doi.org/10.1007/s11852-015-0402-z

BHANAGE, D.A., A.V. PAWAR, AND K. KOTECHA. 2021. IT infrastructure anomaly detection and failure handling: A systematic literature review focusing on datasets, log preprocessing, machine and deep learning approaches, and automated tool. IEEE Access, 9: 156392-156421. http://dx.doi.org/10.1109/ACCESS.2021.3128283.

CHANDER, G., AND B. MARKHAM. 2003. Revised Landsat-5 TM radiometric calibration procedures and postcalibration dynamic ranges. IEEE Transactions on Geoscience and Remote Sensing, 41: 2674-2677. https://doi.org/10.1109/TGRS.2-003.818464.

CHANDER, G., B. MARKHAM, AND D. HELDER. 2009. Summary of current radiometric calibration coefficients for Landsat MSS, TM, ETM+, and EO-1 ALI sensors. Remote Sensing of Environment, 113(5): 893-903. https://doi.org/10.1016/j.rs-e.2009.01.007.

CHOUDHURY, D., K. DAS, AND A. DAS. 2019. Assessment of land use land cover changes and its impact on variations of land surface temperature in Asansol-Durgapur development region. The Egyptian Journal of Remote Sensing and Space Science, 22(2): 203-218. https://doi.org/10.1-016/j.ejrs.2018.05.004.

DARWISH, K. 2024. Monitoring Coastline Dyn-amics Using Satellite Remote Sensing and Geographic Information Systems: A Review of Global Trends. Catrina: The International Journal of Environmental Sciences, 31(1), 1-23. doi: 10.21608/cat.2024.23-3931.1196.

DAS, S., J. PÉREZ-RAMÍREZ, J. GONG, N. DEW-ANGAN, K. HIDAJAT, B.C. GATES, AND S. KAWI. 2020. Core-shell structured catalysts for thermocatalytic, photocatalytic, and electrocatalytic conversion of CO2. Chemical Society Reviews, 49(10): 2937-3004.

EL-BATTRAWY, O., EL-SHELTAWY, A., and HAS-BALLAH, A. 2024. Assessment of Indoor Water-Soluble Particulates in Medical and Residential Sites. Catrina: The International Journal of Envir-onmental Sciences, 32(1), 45-59. doi: 10.21608/c-at.2024.227856.1188.

EL-RAYES, A.E., M.O. ARNOUS, D.R. GREEN, AND N.F. GOUDA. 2023. Geo-hazards assessment of the new-found industrial communities: An example from the 10th of Ramadan industrial region, Egypt. Environmental Systems Research, 12: 21. https://doi.org/10.1186/s40068-023-00306-7

ERDAS. 1999. ERDAS Field Guide, Fifth Edition: Atlanta, GA.

FATHIZAD, H., M. TAZEH, S. KALANTARI, AND S. SHOJAEI. 2017. The investigation of spatio-temporal variations of land surface temperature based on land use changes using NDVI in Southwest of Iran. Journal of African Earth Sciences, 134: 249-256. https://doi.org/10.1016-/j.jafrearsci.2017.06.007

FONSEKA, H., H. ZHANG, Y. SUN, H. SU, AND H. L. LIN. 2019. Urbanization and its impacts on land surface temperature in Colombo metropolitan area, Sri Lanka, from 1988 to 2016. Remote Sensing, 11(8): 957-975. https://doi.org/10.3390/rs11080957

GEBRESLASSIE, H. 2014. Land use-land cover dynamics of Huluka watershed, Central Rift Valley, Ethiopia. International Soil and Water Conservation Research, 2(4): 25-33. https://doi.org/10.1016/S-2095-6339(15)30055-1

GHERRAZ, H., I. GUECHI, AND D. ALKAMA. 2020. Quantifying the effects of spatial patterns of green spaces on urban climate and urban heat island in a semi-arid climate. Bulletin de la Société Royale des Sciences de Liège, 89: 164-185. https://doi.o-rg/10.25518/0037-9565.9821

GOGOI, P.P., V. VINOJ, D. SWAIN, G. ROBERTS, J. DASH, AND S. TRIPATHY. 2019. Land use and land cover change effect on surface temperature over Eastern India. Sci Rep, 20 ; 9 (1) : 8859. https://doi.org/10.1038/s41598-019-45213-z

GONG, A.,Y. CHEN, J. LI, H. GONG, AND X. LI. 2006. Spatial distribution patterns of the urban heat

island based on remote sensing images: A case study in Beijing, China. Journal of the Indian Society of Remote Sensing, 38(4): 654-663. https://doi.org/10.1109/igarss.2006.600

GRIGORAȘ, G., AND B. URIȚESCU. 2019. Land use/land cover changes dynamics and their effects on surface urban heat island in Bucharest, Romania. International Journal of Applied Earth Observation and Geoinformation, 80: 115-126. https://doi.org/1-0.1016/j.jag.2019.03.009

GUHA, S., H. GOVIL, A. DEY, AND N. GILL. 2018. Analytical study of land surface temperature with NDVI and NDBI using Landsat 8 OLI and TIRS data in Florence and Naples City, Italy. European Journal of Remote Sensing, 51(1): 667-678. https://doi.org/10.1080/22797254.2018.1474494

GUHA, S., H. GOVIL, N. GILL, AND A. DEY. 2020. Analytical study on the relationship between land surface temperature and land use/land cover indices. Annals of GIS, 26(2): 201-216. https://doi.org/10.1080/19475683.2020.1754291

HASSAN, Z., R. SHABBIR, S.S. AHMAD, A. H. MALIK, N. AZIZ, A. BUTT, AND S. ERUM. 2016. Dynamics of land use and land cover change (LULC) using geospatial techniques: A case study of Islamabad, Pakistan. SpringerPlus, 5(1): 1–11. https://doi.org/10.1186/s40064-016-2414-z

JABER, S.M. 2019. On the relationship between normalized difference vegetation index and land surface temperature: MODIS-based analysis in a semi-arid to arid environment. Geocarto International, 0(1010–6049): 1–19. https://doi.org/10.1080/10106049.2019.1633421

JANSEN, L.J., AND A. DI GREGORIO. 2002. Parametric land cover and land-use classifications as tools for environmental change detection. Agriculture, Ecosystems & Environment, 91(1-3): 89-100. https://doi.org/10.1016/S01678809(01)-00243-2

JEEVALAKSHMI, D., S. NARAYANA REDDY, AND B. MANIKIAM. 2017. Land surface temperature retrieval from LANDSAT data using emissivity estimation. International Journal of Applied Engineering Research, 12(20): 9679-9687. https://api.semanticscholar.org/CorpusID:40033815

KHYAMI, A. 2021. Impact of land cover change on land surface temperature over Greater Beirut Area–Lebanon. Journal of Geoinformatics & Environmental Research, 2(01): 14-27. https://doi.org-/10.38094/jastt302174

LIU, J.P., A.C. LI, K. H. XU, D.M. VELOZZI, Z.S. YANG, J.D. MILLIMAN, AND D.J. DEMASTER. 2006. Sedimentary features of the Yangtze River-derived along-shelf clinoform in the East China Sea. Marine Geology, 226(3-4): 193-207. https://doi.org/10.1016/j.csr.2006.07.013

MALLICK, J., KANT, Y., AND BHARATH, B. D. 2008. Estimation of Land Surface Temperature Over Delhi Using Landsat-7 ETM+. Journal of Indian Geophysics Union, 12(3), 131-140. https://doi.org/10.1007/s41976-018-0004-2

MENG, Q., W. LIU, L.L. ZHANG, M. ALLAM, Y. BI, X.L. HU, J.F. GAO, D. HU, AND T. JANCsÓ. 2022. Relationships between land surface temperatures and neighboring environment in highly urbanized areas: Seasonal and scale effects analyses of Beijing, China. *Remote Sensing* 14 (17): 4340. https://doi.org/10.3390/rs14174340.

Mostafa, W., Z. Magd, S. Abo Khashaba, B. Abdelaziz, E. Hendawy, A. Elfadaly, M. Nabil, D. Kucher, S. Chen, and E. S. Mohamed. 2023. Impacts of Human Activities on Urban Sprawl and Land Surface Temperature in Rural Areas: A Case Study of El-Reyad District, Kafrelsheikh Governorate, Egypt." Sustainability, 15: 13497. https://doi.org/10.3390/su151813497

MOUBARAK, A.H., ARNOUS, M.O., AND EL-RAYES, A.E. 2021. Integrated Geoenvironmental and Geotechnical Risk Assessment of East Port Said Region, Egypt for Regional Development. Geotechnical and Geological Engineering, 39(2), 1497-1520. http://doi.org/10.1007/S10706-020-01571-4.

NASA. 2003. The Band Designations for the Landsat Satellites. Retrieved from http://landsat.usgs.gov-/using_landsat_7_data.php.6

NASA. 2013. The Band Designations for the Landsat Satellites. Retrieved from http://landsat.us-gs.gov/band.

NETELER, M. 2010. Estimating Daily Land Surface Temperatures in Mountainous Environments by Reconstructed MODIS LST Data. Remote Sensing, 2(1), 333-351. https://doi.org/10.3390/rs1020333

OBIEFUNA, J.N., OKOLIE, C.J., NWILO, P.C., DARAMOLA, O.E., AND ISIOFIA, L.C. 2021. Potential Influence of Urban Sprawl and Changing Land Surface Temperature on Outdoor Thermal Comfort in Lagos State, Nigeria. Quaestiones Geographicae, 40(1), 5-23. https://doi.org/10.2-478/quageo-2021-0001

OKE, T.R. 1982. The energetic basis of the urban heat island. Quarterly Journal of the Royal Meteorological Society 108 (455): 1-24. http://doi.org/10.1002/qj.49710845502.

PAL, S., AND ZIAUL, S.K. 2017. Detection of Land Use and Land Cover Change and Land Surface Temperature in English Bazar Urban Centre. The Egyptian Journal of Remote Sensing and Space Science, 20(1), 125-145. https://doi.org/10.10-16/j.ejrs.2016.11.003

PRATA, A.J., CASELLES, V., COLL, C., SOBRINO, J.A., AND OTTLE, C. 1995. Thermal Remote Sensing of Land Surface Temperature From Satellites: Current Status and Future Prospects. Remote Sensing Reviews, 12(3-4), 175-224. https://doi.org/10.1080/02757259509532285

PUREVDORJ, R., TATELSHI, T., AND ISHIYAMA, Y. 1998. Relationships Between Percent Vegetation Cover and Vegetation Indices. International Journal of Remote Sensing, 19(18), 3519–3535. http://doi.org/10.1080/014311698213795.

SHALABY, H., HERMAS, E., KHORMI, H., FARG-

HALY, A.M., ELSAYED, A.M., ALQURASHI, A., AND ASCOURA, I. 2022. The Interplay Between Spatial Urban Expansion and Morphologic Landscapes East of Cairo, Egypt Using Time Series Satellite Imagery. ISPRS International Journal of Geo-Information, 11(7), 386. https://doi.org/10.3390/ijgi11070386.

SISODIA, P.S., TIWARI, V., AND KUMAR, A. 2014. Analysis of Supervised Maximum Likelihood Classification for Remote Sensing Image. International Conference on Recent Advances and Innovations in Engineering (ICRAIE-2014), 1-4. https://doi.org/10.1109/ICRAIE.2014.6909319

UNITED NATIONS. 2014. World Urbanization Prospects. Retrieved from https://www.un.org/development/desa/en/news/population/world-urbanization-prospects.html.

USGS. 2014. Using the USGS Landsat 8 Product. Retrieved December 11, 2014, from https://landsat.usgs.gov/using-usgs-landsat-8-product.

VAUCLIN, M., VIEIRA, S.R., BERNARD, R., AND HATFIELD, J.L. 1982. Spatial Variability of Surface Temperature Along Two Transects of a Bare Soil. Water Resources Research, 18(6), 1677-1686. https://doi.org/10.1029/WR018i006p01677

VINAYAK, B., LEE, H.S., AND GEDEM, S. 2021. Prediction of Land Use and Land Cover Changes in Mumbai City, India, Using Remote Sensing Data and a Multilayer Perceptron Neural Network-Based Markov Chain Model. *Sustainability*, 13(2), 471. https://doi.org/10.3390/su13020471.

WANG, Y.C., HU, B.K., MYINT, S.W., FENG, C.C., CHOW, W.T., AND PASSY, P.F. 2018. Patterns of Land Change and Their Potential Impacts on Land Surface Temperature Change in Yangon, Myanmar. Science of the Total Environment, 643, 738-750. https://doi.org/10.1016/j.scitotenv.2018.06.209

WENG, Q., LU, D., AND SCHUBRING, J. 2004. Estimation of Land Surface Temperature–Vegetation Abundance Relationship for Urban Heat Island Studies. Remote Sensing of Environment, 89(4), 467-483. https://doi.org/10.1016/j.rse.2003.11.005.

WENG, X.Y., ZHENG, C.J., XU, H.X., AND SUN, J.Y. 2007. Characteristics of Photosynthesis and Functions of the Water–Water Cycle in Rice (Oryza sativa) Leaves in Response to Potassium Deficiency. Physiologia Plantarum, 131(4), 614-621. https://doi.org/10.1111/j.13993054.2007.00978.x

WERE, K., DICK, Ø.B., AND SINGH, B.R. 2014. Exploring the Geophysical and Socioeconomic Determinants of Land Cover Changes in Eastern Mau Forest Reserve and Lake Nakuru Drainage Basin, Kenya. GeoJournal, 79(6), 775–790. https://doi.org/10.1007/s10708-014-9525-2.

XIE, M., WANG, Y., CHANG, Q., FU, M., AND YE, M. 2013. Assessment of Landscape Patterns Affecting Land Surface Temperature in Different Biophysical Gradients in Shenzhen, China. Urban Ecosystems, 16(4), 871-886. https://portal.issn.org/resource/ISSN/1083-8155

XIONG, J., LIU, Y., LIN, X., ZHANG, H., ZENG, J., HOU, J., AND CHU, H. 2012. Geographic Distance and pH Drive Bacterial Distribution in Alkaline Lake Sediments Across Tibetan Plateau. Environmental Microbiology, 14(9), 2457-2466. https://doi.org/10.1111%2Fj.14622920.2012.02799.x

ZHA, Y., GAO, J., AND NI, S. 2003. Use of Normalized Difference Built-Up Index in Automatically Mapping Urban Areas from TM Imagery. International Journal of Remote Sensing, 24(3), 583-594. https://doi.org/10.1080/01431160304987

ZHAO, H.M., AND CHEN, X.L. 2005. Use of Normalized Difference Bareness Index in Quickly Mapping Bare Areas from TM/ETM. Geoscience and Remote Sensing Symposium, 3 (25–29), 1666–1668. https://doi.org/10.1109/IGARSS.2005.1526319.

# تقييم تأثير تغير الغطاء الأرضى على الأختلافات في درجة حرارة سطح الأرض (LST) ، مؤشر الغطاء النباتي (NDVI) ، و مؤشر البناء العمرانى (NDBI) ، باستخدام بيانات الأقمار الصناعية لاندسات في شمال شرق القاهرة، مصر

**مروة عبد العليم محمد[1]، محمد عثمان عرنوس[2]، محمد حلمى جريش[2]، هانى فتحى عبد الجواد[1]**

[1]قسم الجيولوجيا- كلية العلوم - جامعة العريش - العريش - مصر

[2]قسم الجيولوجيا- كلية العلوم - جامعة قناة السويس - الاسماعيلية – مصر

## الملخص العربي

تُعَدُّ مدينة شمال شرق القاهرة في مصر من أحدث المدن الجديدة، حيث شهدت زيادةً وتوسعًا سريعًا في الكثافة العمرانية خلال العقود الأخيرة. لذا، أصبح من الضرورى مراقبة وفهم التداعيات البيئية لتحولات الغطاء الأرضي في مثل هذه المناطق وتأثير هذا التغير على العوامل البيئية لتحقيق التنمية المستدامة والمحافظة على البيئة. فالدراسة الحالية تهدف إلى فهم ودراسة العلاقات المتشابكة المكانية لتقييم تأثير تغير الغطاء الأرضي، الناتج عن الزيادة العمرانية المفاجئة بأنشطتها المختلفة،علي ومؤشر البناء العمرانى (NDBI) ومؤشر الغطاء النباتي (NDVI) ، ومؤشر درجة الحرارة لسطح الأرض (LST) لمنطقة على مدار 20 عامًا (2000-2020) باستخدام صور لأقمار صناعية أمريكية من نوع لاندسات متعددة الفترات الزمنية، مثل صور ETM+ و OLI/TIRS وحيث تم عمل تصنيف لصور الأقمار الصناعية لتضم خمس قنات متميزة تغطى الغطاء الأرضي لمنطقة الدراسة وهى المناطق الحضرية، والأراضي الجرداء، والمناطق الزراعية، والتربة المملحة، والمسطحات المائية..وكشفت النتائج عن زيادة المناطق العمرانية بحوالى 211.2 كيلومتر مربع، بينما تقلصت الأراضي القاحلة والمناطق الزراعية بمقدار 196.2 كيلومتر مربع و 23.9 كيلومتر مربع على التوالي و سجلت أعلى قيم لدرجة حرارة سطح الأرض في الأراضي القاحلة من 38-45 درجة مئوية في عام 2000 إلى 61-62 درجة مئوية في عام 2020، بينما تراوحت درجات الحرارة في المناطق العمرانية من 36-37 درجة مئوية في عام 2000 إلى 60 درجة مئوية في عام 2020 . وأستنتج أن زيادة المساحات العمرانية هي السبب الرئيسي لزيادة درجة حرارة سطح الأرض ، كما لوحظ أن درجة حرارة سطح الأرض تتناسب طرديًا مع مؤشر البناء الحضري (NDBI) وتتناسب عكسيًا مع مؤشر الغطاء النباتي(NDVI) ، وتوضح النتائج أهمية تقييم تأثير العمران السريع على البيئة وأهمية التخطيط الحضري وزيادة المساحات الخضراء لتحقيق التنمية المستدامة .